# INFLUENCE OF THE MORPHOLOGY ON MELTING KINETICS OF NANOCOMPOSITES

**R.V. DINZHOS, N.A. REKHTETA, E.G. PRIVALKO**[1]

**V.O. Sukhomlynskyi Mykolaiv State University**
*(24, Nikolska Str., Mykolaiv 54030, Ukraine; e-mail: dinzhos@mail.ru),*

[1]**Institute of Macromolecular Chemistry, Nat. Acad. Sci. of Ukraine**
*(48, Kharkiv Rd., Kyiv 02160, Ukraine)*

UDC 538.91+536.6
©2007

Specimens of a pure polyamide 6 (PA6) homopolymer and a number of commercial polymer nanocomposites (PNCs) containing up to 7.5 wt.% of exfoliated organoclay nanoparticles fabricated by crystallizing them under non-isothermal conditions have been studied at room temperature by the wide- and small-angle X-ray scattering (WAXS and SAXS) methods. The melting behavior of the specimens has also been studied making use of temperature-modulated differential scanning calorimetry (TMDSC) at three underlying heating rates and five modulation frequencies. The $\alpha$- and $\gamma$-modifications of PA6 crystals were found to be independently formed from the melt during its cooling, with their content ratio ($\alpha/\gamma$) tending to grow as the organoclay content or the cooling rate becomes higher. Organoclay platelets strongly scattered in the PNC were demonstrated to become spatially ordered into two different fractal-like structures (mass fractals) with the characteristic structural scales of 5–14 and 14–100 nm. The melting endotherm profiles for pure PA6 and a PNC were found to be described by a simple Debye's model with a single corresponding characteristic time dependent on the temperature and the underlying cooling rate. The mechanisms of structural rearrangements in the melting intervals of pure PA6 and a PNC turned out practically identical. However, the spatial scale of such rearrangements in the PNC proved to be significantly smaller, owing to the presence of considerable steric constraints imposed by the infinite cluster of nanoparticles onto the mobility of PA6 chains in the melt.

## 1. Introduction

The solid state of polymers crystallizing at a temperature below the "equilibrium" melting one, $T_m^0$, is unique in the sense that a significant portion of material, namely, $1 - X$, where $X$ is the crystallinity degree, remains in a disordered non-crystalline state; in general, the latter is characterized by missed loops on the end surface of the crystal with folded chains (lamellae), as well as by the presence of chain ends and "entangled" chains in the interlamellar space [1–3]. Such explicit violation of the Gibbs phase rule for a thermodynamically equilibrium system is a confirmation of the fact that the lamellar morphology for such "partially crystalline" polymers is not in nonequilibrium, being metastable.

The implementation of the TMDSC technique in the early 1960s made it standard for the express analysis of a metastable state of partially crystalline polymers, because it allows a reduction of the corresponding melting temperature $T_m$ with respect to $T_m^0$ and a corresponding reduction $\Delta H_m^*$ of the melting heat with respect to the melting enthalpy of a perfect crystal $\Delta H_m^0$ to be measured. Moreover, the qualitative information concerning the internal morphology of a partially crystalline polymer can be obtained from the shape of melting endotherms at the heating of polymers in the DSC regime [4] at a rate higher than that of characteristic structural transformations, i.e., under condition of "zero-entropy production" [5]. However, the expected behavior of melting endotherms can be distorted by the contributions of other endo- and exothermal effects, such as "cold crystallization", local melting and recrystallization, overheating, and so on [6,7]. Nevertheless, such effects can be adequately taken into account by either making use of the TMDSC regime, which separates the reversible and irreversible contributions to the specific heat [8–10], or analyzing the frequency and underlying heating rate dependences of the heat capacity [11–14].

Our previous studies of the series of isotactic polypropylene (PP) and PP/aerosil nanocomposites

carried out in the framework of the TMDSC method [15] demonstrated that a simple Debye's model [11–14] is valid, at a semiquantitative level, for melting endotherms of both pure PP and nanocomposites. In this work, the same approximation was used to describe the melting behavior of another series of PNCs, namely, PA6/organoclay.

## 2. Experimental Part

Pure PA6 (marked by a supplier as 200A) and three nanocomposites (299F, 299E, and 299D) were fabricated by mixing the melt of 200A with 2.5, 5.0, and 7.5%, respectively, of hybrid organoclay in an extruder. Organoclay (montmorillonite) was used as a filler; it is a typical representative of layered silicates with a stack-type structure and a very large length-to-thickness ratio: the thickness of a separate plate is 1 nm, while its length is from 100 to 1000 nm; the specific surface is about 760 $m^2/g$. Montmorillonite used for fabricating nanocomposites was modified with organic ions with hydrophobic tails.

Solid specimens fabricated under the same conditions of non-isothermal crystallization from a melt had been studied earlier [17, 18] at room temperature by the WAXS and SAXS methods. Analogous specimens had been studied making use of the standard DSC method at their heating in the temperature interval 220–500 K and at a rate of 10 K/min.

Enthalpy relaxation in the course of heating was studied on a Perkin Elmer DSC-2 calorimeter, modernized and supplied with a software for signal processing (IFA Gmb, Ulm) in the temperature-modulated (TM) regime. Every specimen was preliminarily "overheated" to a temperature of approximately 50 K above the equilibrium melting temperature of PA6 ($T_m \approx 490$ K), held at this temperature for 3 min, cooled in the DSC regime at either of two constant cooling rates $q^- = 20$ or 0.5 K/min to 400 K, held at this temperature for 2 min once more, and heated up again immediately in the TMDSC regime at one of three main heating rates $q^+ = 0.5$, 1, or 2 K/min; the amplitude of modulation was 0.1 K; and the modulation frequencies $f = 10$, 17, 33, 50, and 100 mHz. Calibration measurements for the determination of the specific heat $c_p$ and its reversible part, i.e. the complex specific heat $c_p^*$, were carried on according to the requirements described in works [19,20] and using sapphire and quartz as standards.

## 3. Results and Their Discussion

### *3.1. Structural characteristic of initial specimens*

Rather intensive reflections at scattering angles $2\theta \approx 20.0$ and 23.8° were the main characteristic feature of the WAXS diagrams for a 200 A specimen cooled from the melt at the rate $q^- = 0.5$ K/min (Fig. 1,*a*). Similar reflections were observed in the WAXS diagrams for an analogous specimen cooled from the melt at the rate $q^- = 20$ K/min (Fig. 1,*b*), although their intensity became considerably reduced. This evidences for the availability of the monoclinic ($a$) crystal phase with hydrogen bonds between antiparallel chains [21–23] in pure, partially crystalline PA6. The crystallinity degree $X_{\mathrm{WAXS}}$ calculated from WAXS data following the standard procedure [20] appeared to be less than 30% for both specimens, with the average error of 4% (see Table 1).

Two main reflections, which are typical of $\alpha$-modifications of crystals, can be observed on PNC WAXS diagrams as either auxiliary peaks (Fig. 1,*a*) or shoulders (Fig. 1,*b*) in the vicinity of the main diffraction maximum at $2\theta \approx 21.4°$. This maximum, together with an auxiliary reflection at $2\theta \approx 10.5°$, evidences for a pseudohexagonal (or monoclinic) crystal lattice with hydrogen bonds between parallel chains (a $\gamma$-modification) [21–23]. Hence, the $\alpha$- and $\gamma$-modifications of the PA 6 crystal are formed from the melt independently during its cooling; the ratio between the contents of $\alpha$- and $\gamma$-modifications reveals a tendency to a reduction with increase in either the organoclay content or the cooling rate, although the $X_{\mathrm{WAXS}}$-values for the polymeric matrices were almost identical to all the specimens of this series (Table 1).

In the vicinity of the scattering vector $q = (4\pi/\lambda)\sin\theta \approx 0.37$ $\mathrm{nm}^{-1}$, which corresponds to the Bragg periodicity $D = 2\pi/q \approx 17.0$ nm, the SAXS diagrams for a 200 A specimen crystallized from the melt

**T a b l e 1. Melting heats and crystallinity degrees**

| Specimen | $X_{\mathrm{WAXS}}$ | $X_{\mathrm{DSC}}$ | $\Delta H_m^*$, J/g |
|---|---|---|---|
| $q^- = 0,5$ K/min | | | |
| 200A | 0.26 | 0.25 | 57.5 |
| 299F | 0.33 | 0.31 | 71.3 |
| 299E | 0.35 | 0.33 | 75.9 |
| 299D | 0.29 | 0.28 | 64.4 |
| $q^- = 20$ K/min | | | |
| 200A | 0.21 | 0.20 | 46.0 |
| 299F | 0.26 | 0.24 | 55.2 |
| 299E | 0.29 | 0.27 | 62.1 |
| 299D | 0.23 | 0.21 | 48.3 |

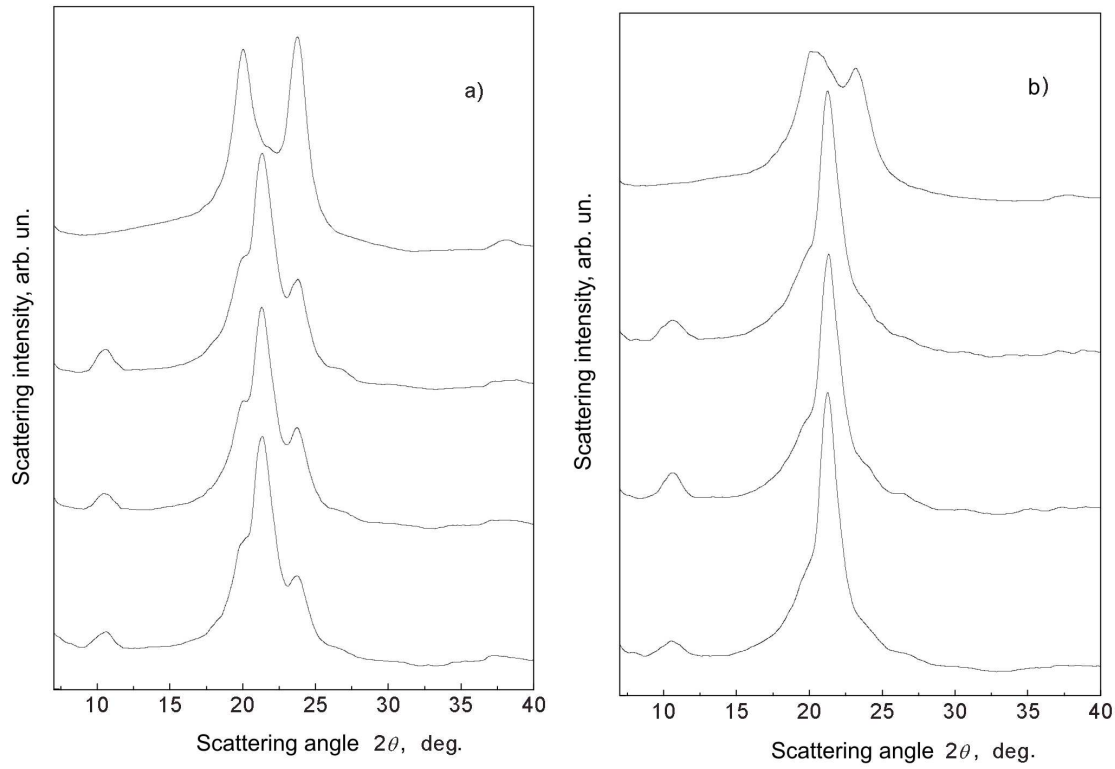


Fig. 1. WAXS diagrams for specimens 200A, 299F, 299E, and 299D (from top to bottom) crystallized by cooling from the melt at the rate $q^- = 0.5$ ($a$) and 20 K/min ($b$)

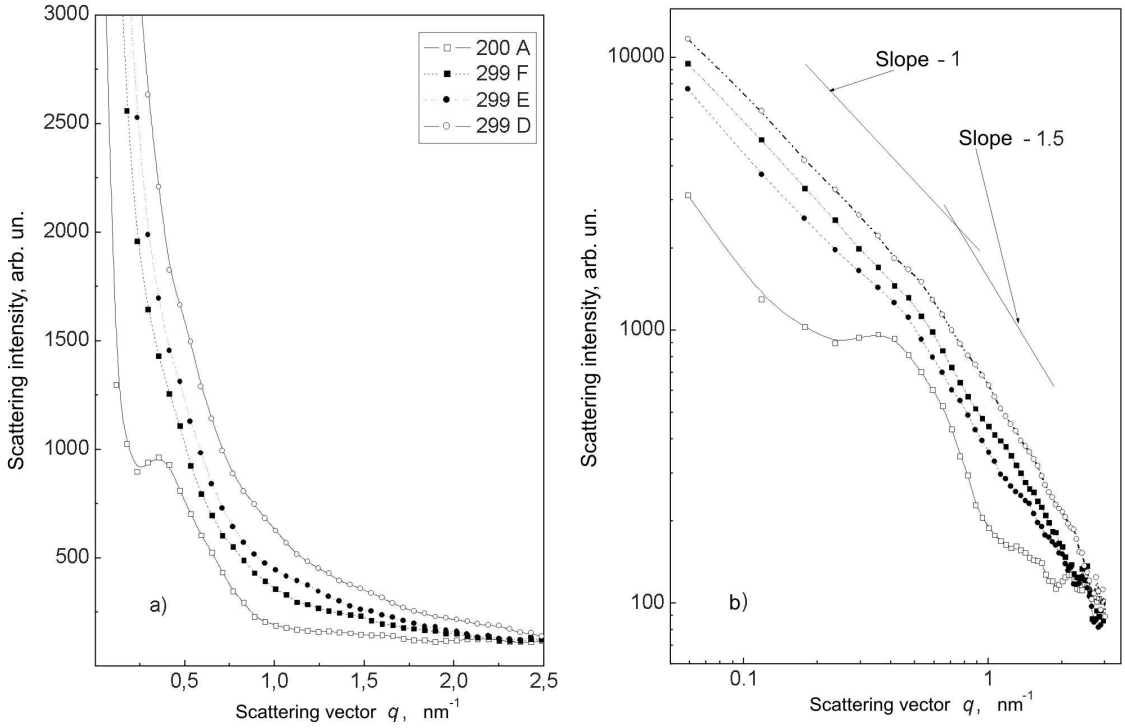


Fig. 2. SAXS diagrams in linear ($a$) and log-log coordinates ($b$)

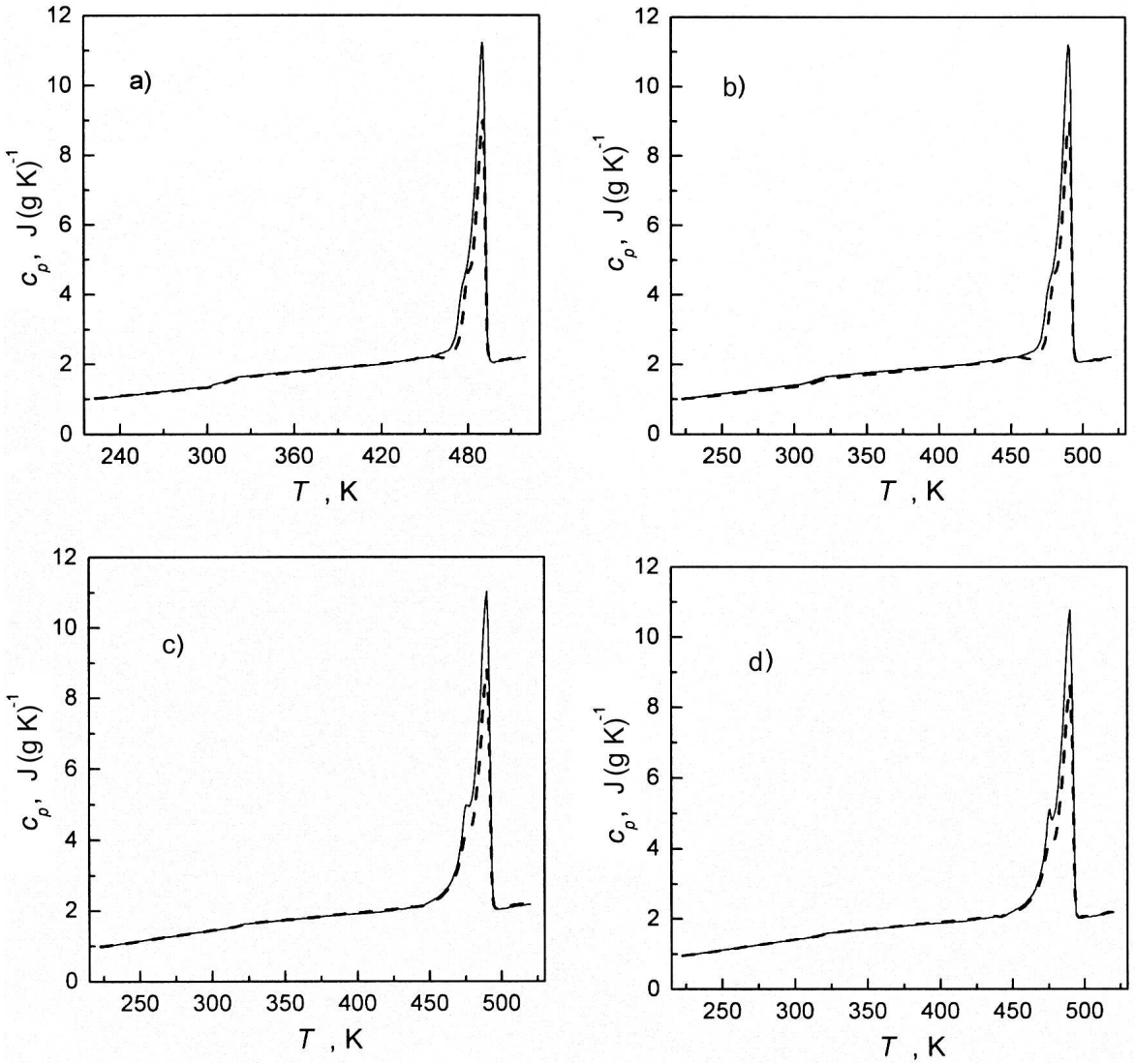


Fig. 3. Thermograms of heating in the standard DSC regime for specimens 200A ($a$), 299F ($b$), 299E ($c$), and 299D ($d$) crystallized by cooling from the melt at the rate $q^- = 0.5$ (solid) and 20 K/min (dashed curves)

at the rate $q^- = 0.5$ K/min (Fig. 2,$a$) are typical of a disordered, partially crystalline polymer with crystallite inclusions, folded-chain lamellae being separated by non-crystalline spaces [21]. Those reflections cannot be observed in standard SAXS curves for PNCs, because the SAXS intensity increases very strongly with increase in the organoclay content if the scattering vector falls within this range (Fig. 2,$a$). However, if those data are plotted on the log–log scale (Fig. 2,$b$), the presence of at least two linear sections with different slopes at $q$'s larger and smaller than $q^*$ testifies that organoclay particles are spatially arranged into the fractal-like structures of two types [17, 25]. This means that, if the scattering vector amplitude lies between the so-called "Guinier regime" (small $q$-values) and the "Bragg regime" (large $q$-values), the dependence of the SAXS intensity $I(q)$ corresponds to the scaling relation

$$I\ (q)\ \sim\ q^{-\alpha}, \tag{1}$$

where the power exponent $\alpha$ characterizes the type of scattering object [25]. Proceeding from rather small values of the parameter $\alpha$ in the vicinity of the overlapping point $q^* = 0.45 \div 0.50$ nm$^{-1}$ (Fig. 2,$b$), one can distinguish the regimes of scattering by the mass

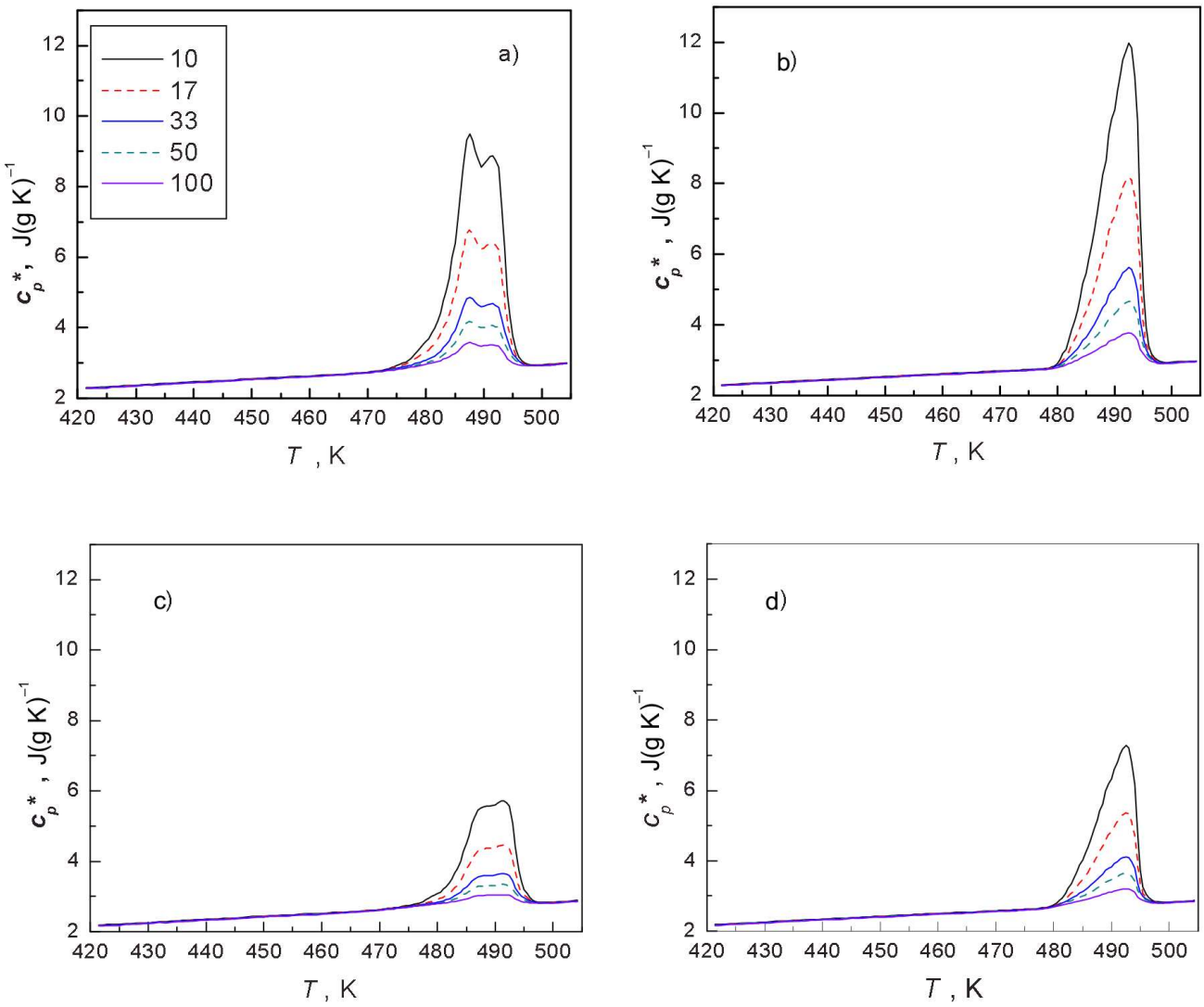


Fig. 4. Complex specific heat for specimens 200A ($a$ and $b$) and 299D ($c$ and $d$) crystallized by cooling from the melt at the rate $q^- = 0.5$ ($a$ and $c$) and 20 K/min ($b$ and $d$) and heated at the rate $q^+ = 20$ K/min

fractal in the structural dimension ranges of 14–100 (at $q < q^*$) and 5–14 nm (at $q > q^*$).

Each specific heat reveals a corresponding jump $\Delta c_p$ at the vitrification temperature $T_g \approx 308$ K of a continuous amorphous PA6 matrix and substantial endothermal melting effects ($\Delta H_m^*$), with a maximum at $T_m \approx 492$ K, for the crystalline PA6 nanophase; the latter are appreciable in thermograms for 200 A specimens crystallized from the melt at two different rates (Fig. 3,$a$). The thermograms of PNC heating (Figs. 3,$b$–$d$) are similar in general, but the magnitude of the jump $\Delta c_p$ diminishes with increase in the organoclay content. The value of $\Delta H_m^*$ – and, accordingly, the crystallinity degree calculated using the DSC data, $X_{\rm DSC} = \Delta H_m^*/\Delta H_m$, where $\Delta H_m = 230$ J/g is the melting enthalpy for a perfect crystal with $\alpha$-modifications [21] – becomes a little smaller with increase in the preliminary cooling rate $q^-$ (Table 1).

### *3.2. Melting kinetics*

The plots of the temperature dependence of the complex specific heat $c_p^*$ (Fig. 4) demonstrate that the melting endotherms of specimens cooled at the rate $q^- = 20$ K/min $\gg q^+$ (hereafter referred to as series 2) were unimodal, having a single maximum at the

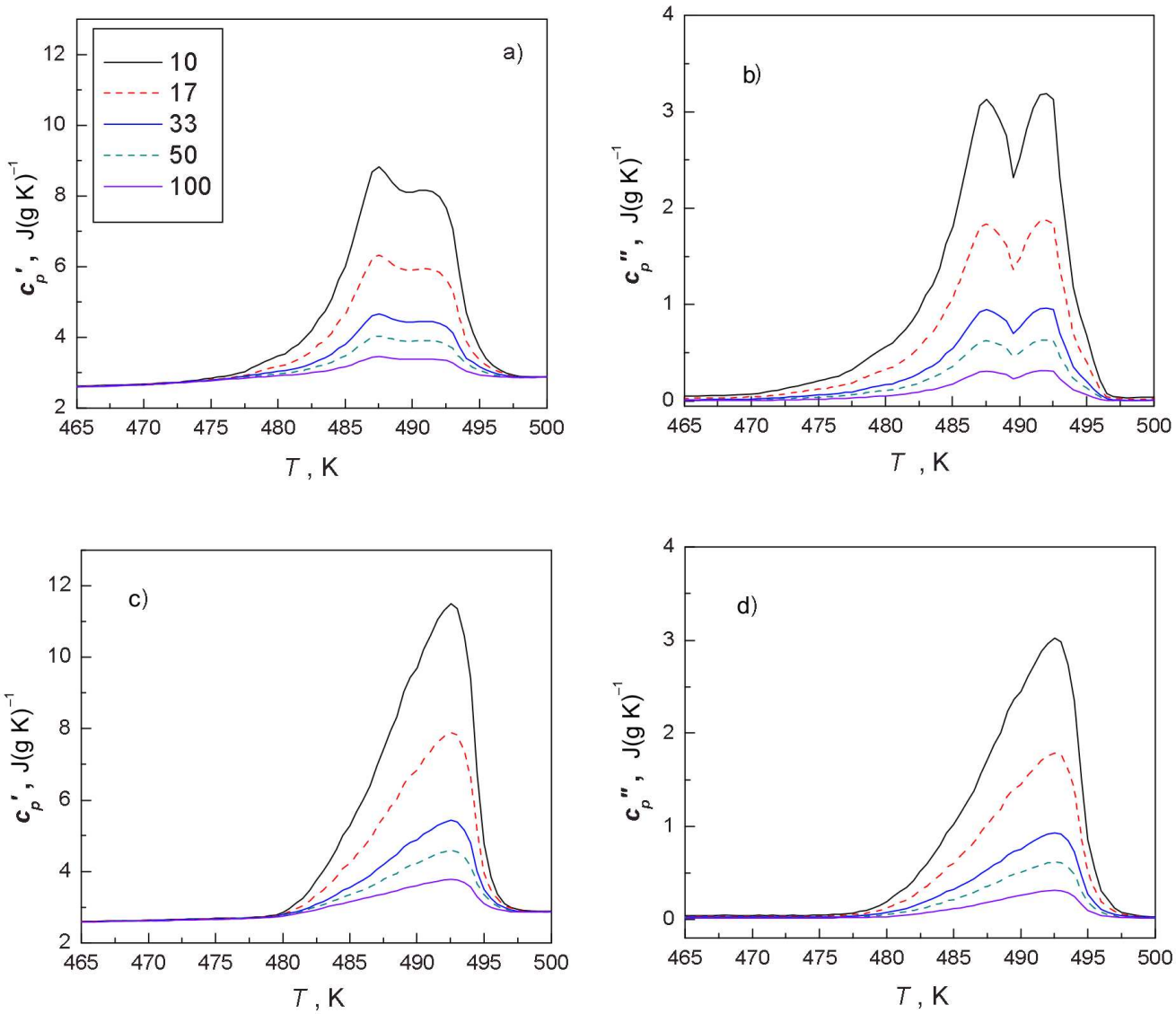


Fig. 5. Real ($a$ and $c$) and imaginary ($b$ and $d$) components of the complex specific heat for specimens 200A ($a$ and $b$) and 299F ($c$ and $d$) crystallized by cooling from the melt at the rate $q^- = 0.5$ K/min and heated at the rate $q^+ = 0.5$ K/min

corresponding melting temperature $T_m$. At the same time, in analogous plots for specimens fabricated by cooling at the rate $q^- = 0.5$ K/min $\leq q^+$ (series 1), one can observe not only the main melting peak at $T_m$, but an auxiliary maximum at $T'_m < T_m$. It is most probable that the discrepancies between melting endotherms reflect the dependence of the relative content of $\alpha$- and $\gamma$-modifications in pure PA6 and PNC crystals on the heating rate (see work [16] and the discussion above).

The reversible specific heats $c_p^*$, considered beyond the melting temperature range, are predictably independent of the modulation frequency, although the value of $c_p^*$ and the areas under peaks decrease here with increase in the modulation frequency (Fig. 4). The same behavior was observed for the real ($c'_p$) and imaginary ($c''_p$) components of the complex specific heat $c_p^* = c'_p - ic''_p$ (Fig. 5). These results testify that the characteristic times $\tau$ of structural transformations and the modulation periods, i.e. the inverse frequencies, were comparable. Considerably smaller values of $c_p^*$ for PNC can be attributed to some steric constraints imposed on the chain mobility of PA6 in the melt state by the infinite cluster of nanoparticles [15].

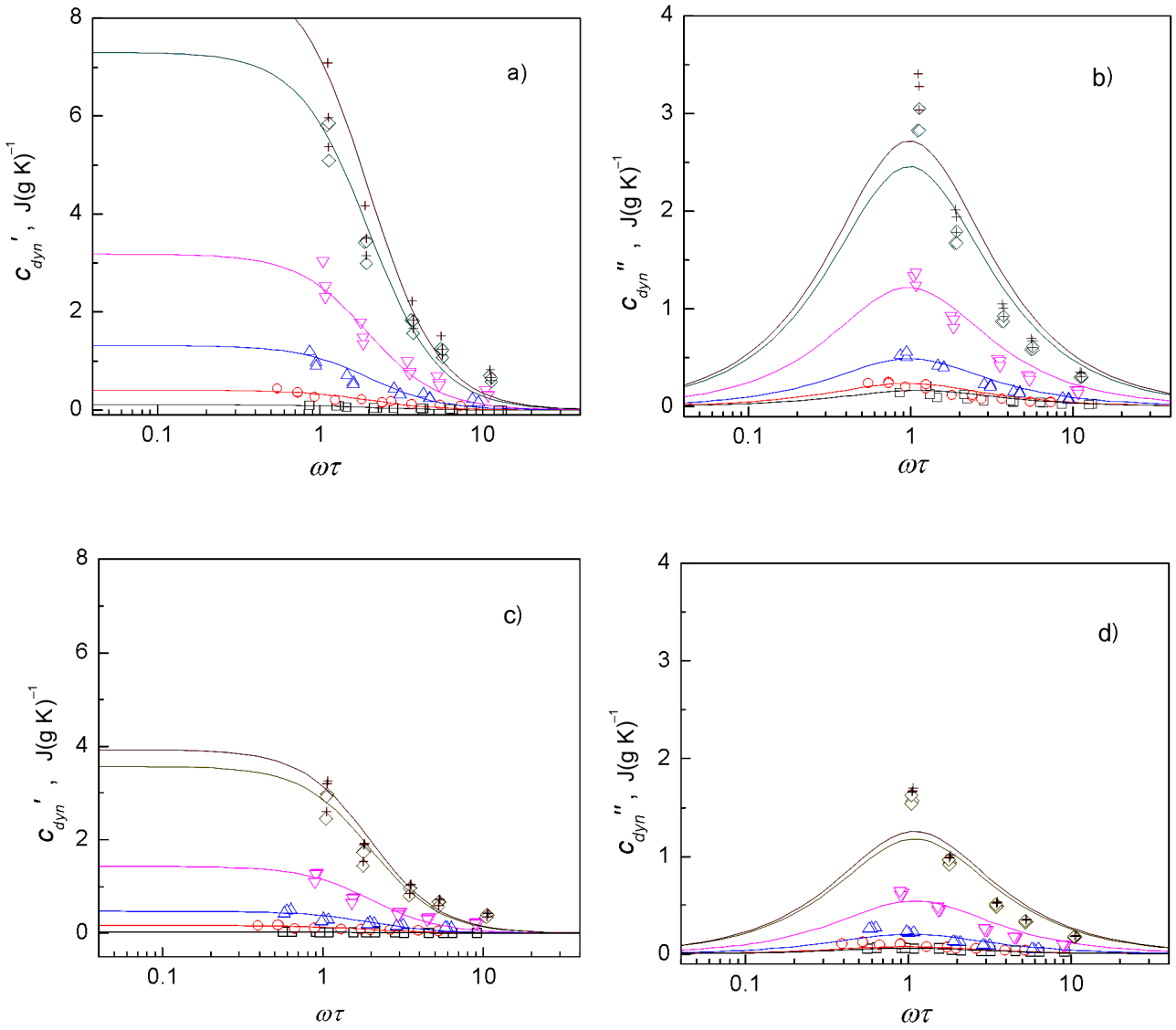


Fig. 6. Debye's diagrams for real ($a$ and $c$) and imaginary ($b$ and $d$) components of the complex specific heat at a temperature of 475 (squares), 478 (circle), 481 (deltas), 484 (nablas), 487 (diamonds), and 490 K (crosses) for specimens 200A ($a$ and $b$) and 299D ($c$ and $d$) crystallized by cooling from the melt at the rate $q^- = 0.5$ K/min

The corresponding values of the dynamic parts of the real and imaginary components of $c_p^*$ ($c'_{\rm dyn}(\omega)$ and $c''_{\rm dyn}(\omega)$, respectively) are expressed as follows:

$$c'_p(\omega) = c_{\rm st} + c'_{\rm dyn}(\omega), \tag{2a}$$

$$c''_p(\omega) = c''_{\rm dyn}(\omega), \tag{2b}$$

which describe the response to the cyclic modulation frequency $\omega$ in the melting interval. Following Debye [11–14], we write down this response in the form

$$c^*_{\rm dyn}(\omega) = c'_{\rm dyn}(\omega) - ic''_{\rm dyn}(\omega) =$$

$$HF/(1+i\omega\tau) = HF(1-i\omega\tau)/(1+i\omega\tau)(1-i\omega\tau) =$$

$$\zeta_0\tau/(1+\omega^2\tau^2) + i\zeta_0\omega\tau^2/(1+\omega^2\tau^2), \tag{3a}$$

$$c'_{\rm dyn}(\omega) = c'_p(\omega) - c_{\rm st} = \zeta_0\tau/(1+\omega^2\tau^2), \tag{3b}$$

$$c''_{\rm dyn}(\omega) = \zeta_0 \omega\tau^2/(1+\omega^2\tau^2), \qquad (3c)$$

where $HF = \tau\zeta_0$ is the thermal flow rate, $\tau$ the characteristic time, and $\zeta_0$ the structural transformation rate.

The experimental values of $c'_{\rm dyn}(\omega)$ and $c''_{\rm dyn}(\omega)$ at three main heating rates were calculated by Eqs. (3b) and (3c), and the obtained approximation values of $\zeta_0$ and $\tau$ were used for plotting the Debye dependences (the $c'_{\rm dyn}(\omega)$-values were obtained from Eq. (3b) assuming that the constant component $c_{\rm st}$ is described by a straight base line connecting the start and end points of the melting endotherm in Fig. 5). The frequency-dependent diagrams of melting endotherms (Fig. 6) for all studied specimens can be described semiquanitatively by a simple Debye's model. Considerable deviations of points can testify that the approximation parameters $\zeta_0$ and $\tau$ are averaged over no less than two overlapping mechanisms of structural transformations, i.e. melting of $\alpha$- and $\gamma$-modifications of crystals.

**T a b l e 2. Characteristic times (in seconds) of structural transformations in various specimens in their melting intervals**

| $T$, K | $q^-/q^+$ | | | | | |
|---|---|---|---|---|---|---|
| | 0.5/0.5 | 0.5/1.0 | 0.5/2.0 | 20/0.5 | 20/1.0 | 20/2.0 |
| | | | 200A | | | |
| 475 | (126) | (126) | (86) | ... | ... | ... |
| 478 | 73 | 73 | 55 | 67 | 46 | 48 |
| 481 | 94 | 94 | 87 | 59 | 56 | 64 |
| 484 | 108 | 108 | 105 | 94 | 93 | 89 |
| 488 | 113 | 113 | 110 | 108 | 108 | 106 |
| 491 | 113 | 113 | 111 | 111 | 111 | 110 |
| | | | 299F | | | |
| 475 | (114) | (97) | (116) | ... | ... | ... |
| 478 | 69 | 65 | 70 | 67 | 39 | 58 |
| 481 | 84 | 95 | 91 | 59 | 58 | 56 |
| 484 | 103 | 108 | 107 | 94 | 94 | 85 |
| 488 | 111 | 112 | 111 | 108 | 108 | 105 |
| 491 | 111 | 113 | 112 | 111 | 111 | 109 |
| | | | 299E | | | |
| 475 | (70) | (77) | (76) | ... | ... | ... |
| 478 | 50 | 56 | 64 | 52 | 35 | 86 |
| 481 | 73 | 80 | 90 | 36 | 50 | 58 |
| 484 | 94 | 100 | 103 | 72 | 74 | 77 |
| 488 | 106 | 109 | 111 | 99 | 99 | 101 |
| 491 | 106 | 110 | 111 | 105 | 106 | 107 |
| | | | 299D | | | |
| 475 | (56) | (64) | (91) | ... | ... | ... |
| 478 | 40 | 53 | 52 | 94 | 44 | 70 |
| 481 | 58 | 59 | 63 | 51 | 42 | 44 |
| 484 | 89 | 90 | 93 | 68 | 67 | 68 |
| 488 | 104 | 105 | 106 | 97 | 96 | 97 |
| 491 | 105 | 106 | 107 | 104 | 103 | 103 |

Identical values of the characteristic time for pure PA6 and PNC (Table 2) evidence for identical mechanisms of basic structural transformations in those two polymers, while the $c'_{\rm dyn}(\omega)$- and $c''_{\rm dyn}(\omega)$-values for PNC (Fig. 6), which are several times smaller, as well as the parameter $\zeta_0$ from Eqs. (3b) and (3c), testify to a significant reduction of the spatial scale of such transformations in the latter.

## 4. Conclusions

1. Both modifications ($\alpha$ and $\gamma$) of PA6 crystals are independently crystallized from the melt during its cooling, and the ratio between their contents ($\alpha/\gamma$) decreases as the organoclay content or the cooling rate increases.

2. Organoclay particles, which are strongly dispersed in PNC, form two different fractal-like (similar to a mass fractal) spatial structures in the ranges of characteristic dimensions of 14–100 and 5–14 nm.

3. The behavior of melting endotherms of pure PA6 and PNC can be characterized at a semiquantitative level by a simple Debye's model with a single characteristic time which depends on the temperature and the cooling rate.

4. The mechanisms of structural transformations in pure PA6 and PNC are, in general, identical in their melting interval; however, the spatial scale of transformations in PNC is considerably reduced owing to steric constraints on the mobility of PA6 chains in the melt imposed by the infinite cluster of nanoparticles.


1. P.H. Geil, *Polymer Single Crystals* (Interscience, New York, 1963).
2. A. Keller, Rep. Prog. Phys. **31**, 623 (1968).
3. J.D. Hoffman, G.T. Davis, and J.I. Lauritzen, in *Treatise on Solid State Chemistry, Vol. 3*, edited by N.B. Hannay (Plenum Press, New York, 1976), p. 497.
4. H.-G. Kilian, Prog. Coll. Polymer Sci. **72**, 60 (1986).
5. B. Wunderlich, *Macromolecular Physics, Vol. 3: Crystal Melting* (Academic Press, New York, 1980).
6. V.A. Bershtein and V.M. Egorov, *Differential Scanning Calorimetry in the Physical Chemistry of Polymers* (Khimiya, Leningrad, 1990) (in Russian).
7. B. Wunderlich, Prog. Polymer Sci. **28**, 383 (2003).
8. W.G. Kampert and B.B. Sauer, Polymer **42**, 8703 (2001).
9. Z. Qiu, M. Komura, T. Ikehara, and T. Nishi, Polymer **44**, 7781 (2003).
10. C.-L. Wei, M. Chen, and F.-E. Yu, Polymer **44**, 8185 (2003).
11. J.E.K. Schawe and E. Bergmann, Thermochim. Acta **304–305**, 179 (1997).

12. J.E.K. Schawe and W. Winter, Thermochim. Acta **330**, 85 (1999).

13. A. Toda, C. Tomita, and M. Hikosaka, J. Thermal Anal. **54**, 623 (1998).

14. A. Toda, C. Tomita, M. Hikosaka, and Y. Saruyama, Thermochim. Acta **324**, 95 (1998).

15. V.P. Privalko, R.V. Dinzhos, and E.G. Privalko, J. Macromol. Sci. B **41**, 485 (2004).

16. R.V. Dinzhos, E.G. Privalko, and V.P. Privalko, J. Macromol. Sci. B **44**, 421 (2005).

17. V.P. Privalko, V.M. Karaman, E.G. Privalko, R. Walter, K. Friedrich, M.Q. Zhang, and M.Z. Rong, J. Macromol. Sci. B **41**, 485 (2002).

18. V.M. Karaman, Ph.D. thesis, Institute of Macromolecular Chemistry, National Academy of Sciences of Ukraine, Kyiv, 2003.

19. B. Wunderlich, A. Boller, I. Okazaki, and K. Ishikiriyama, Thermochim. Acta **304–305**, 125 (1997).

20. M. Ribeiro and J.-P.E. Grolier, J. Thermal Anal. Calorimetry **57**, 253 (1999).

21. B. Wunderlich, *Macromolecular Physics, Vol. 1: Crystal Structure, Morphology, Defects* (Academic Press, New York, 1973), Chap. 4.

22. J.P. Parker and P.J. Lindenmeyer, J. Appl. Polymer Sci. **21**, 821 (1977).

23. A.Sh. Goikhman, V.I. Kirichenko, S.S. Demchenko, N.P. Matsibora, and V.P. Privalko, Vysokomol. Soed. A **24**, 43 (1982).

24. V.P. Privalko, V.M. Karaman, E.G. Privalko, B. Lehmann, and K. Friedrich, J. Macromol. Sci. B **42**, 975 (2003).

25. G. Beaucage, J. Appl. Crystallogr. **29**, 134 (1996).

Received 28.12.06.
Translated from Ukrainian by O.I. Voitenko

ВПЛИВ МОРФОЛОГІЇ НА КІНЕТИКУ ПЛАВЛЕННЯ НАНОКОМПОЗИТІВ

*Р.В. Дінжос, М.А. Рехтета, Е.Г. Привалко*

Р е з ю м е

Неізотермічно закристалізовані зразки чистого гомополімеру поліаміду 6 (ПА6) та серії комерційних нанокомпозитів (ПНК), які містять до 7,5 мас.% ексфолійованих наночастинок органоглини, були досліджені при кімнатній температурі методами ширококутового та малокутового рентгенівського розсіяння. Їх плавлення було досліджено температурно-модульованою ДСК (ТМ ДСК) при трьох основних швидкостях нагрівання та п'яти частотах модуляції. Показано, що $\alpha$- та $\gamma$-модифікації кристалів утворюються незалежно під час охолодження з розплаву, відношення вмісту $\alpha$-модифікації до вмісту $\gamma$-модифікації має тенденцію до зростання із збільшенням вмісту органоглини або швидкості охолодження. Розгалужена структура пласких частинок органоглини в ПНК впорядкована в дві різні фракталоподібні (масові фрактали) структури у діапазоні структурних шкал 100–14 та 5–14 нм. Графіки ендотерм плавлення для чистого ПА6 та ПНК можуть бути охарактеризовані простою моделлю Дебая із одним характеристичним часом, який залежить від температури та швидкості охолодження. Механізми структурних перебудов в інтервалі плавлення для чистого ПА6 та ПНК є загалом однакові; однак просторова шкала цих перебудов для ПНК є значно меншою, оскільки існують значні стеричні перешкоди для рухливості ланцюгів ПА6 в розплаві з боку нескінченного кластера наночастинок.